RSC Advances

ROYAL SOCIETY OF CHEMISTRY

www.rsc.org/advances

Simultaneous removal of Methylene blue and Pb^{2+} ion using Ruthenium nanoparticle-loaded activated carbon; Response surface methodology

H. Mazaheri[a], M. Ghaedi[a]*, S. Hajati[b], K. Dashtian[a], M. K. Purkait[c]

[a] *Chemistry Department, Yasouj University, Yasouj, 75918-74831, Iran*

[b] *Department of Physics, Yasouj University, Yasouj, 75918-74831, Iran*

[c] *Department of Chemical Engineering, Indian Institute of Technology Guwahati, Guwahati – 781039, Assam, India.*

---

* Corresponding author Tel./Fax: +98 74 33223048; E-mail: m_ghaedi@mail.yu.ac.ir

---

Abstract

The Ruthenium nanoparticles were synthesized in a green approach with high yield in the presence of ultrasound and then the product was loaded on activated carbon. The characterizations were performed using different techniques such as SEM, XRD, and BET. The simultaneous removal of methylene blue (MB) and Pb^{2+} ions from aqueous solution by Ruthenium nanoparticles loaded on activated carbon (Ru-NPs-AC) was studied. The effects of variables such as initial dye and Pb^{2+} ion concentrations (mg L^{-1}), adsorbent doses (g) and contact time (min) on the simultaneous removal of MB and Pb^{2+} ions were studied. Experiments were conducted using central composite design (CCD) and the optimum experimental conditions were found under response surface methodology (RSM). Adsorption equilibrium data were well fitted by Langmuir isotherm model than Freundlich, Temkin and Dubinin–Radushkevich. Experimental adsorption data were analyzed using various kinetic models such as pseudo- first and second order, Elovich and intraparticle diffusion models. A good fit to pseudo-second order model was observed. Dye removal was varying from 77% to 99% within the operating conditions considered herein.

Keyword: Ruthenium nanoparticles; Methylene blue; Pb^{2+} ion; ultrasound; adsorption.

1. Introduction

The effluents containing dyes are highly toxic for the aquatic media and organisms by influencing on the symbiotic process that affect and disturb the natural equilibrium. The entrance of dyes to environment leads to the decrease in photosynthesis activity and significant change in abundance of different species [1-3]. Effluents coming out from paints, textile and paper industries contain methylene blue and Pb^{+2}. Surface water becomes toxic in presence of dye and Pb^{+2}, toxic nature of which has a severe environmental impact. This has resulted in the enforcement of stringent laws for the maximum allowable limits of their discharge into the open landscapes and water bodies. Pb^{2+} and its compound are highly consumed for storage of battery manufacturing, printing, pigments, fuels, photography material and explosive manufacturing. Even small amount of this element and its compounds is neurotoxin that leads to cancer, anemia and other health problem [2, 3].

The conventional techniques used for simultaneous and competitive removal of dyes and metal ions have high cost while they have medium efficiency to remove hazardous material in sequential steps. Nanoparticles have distinguished physicochemical properties such as high surface reactive center, high mechanical strength, electrical and thermal conductivity compared to the corresponding bulk material [4-8]. The widespread applications of nanoparticles are due to their distinguished remarks including (i) easy synthesis protocol, (ii) high adsorption capacity and (iii) high specific surface area to trap and adsorb pollutants and target species [9-13]. Due to the complex nature of textile effluent, variability of the dyeing process and presence of various amounts of pollutants such as dye and heavy metal ions, very few processes were reported to achieve safe and clean textile wastewater containing multi component target species for the adsorption [14-15]. Conventional and classical methods of studying a process based on the maintenance of other factors at an unspecified constant level neglect the variables interaction, while suffer from drawback such as tedious and labor intensive (requires a number of experiments) to find optimum levels. These limitations are strongly resolved following the application of statistical experimental design such as response surface methodology (RSM) [6]. RSM enables the researchers to estimate relative significance of several affecting factors even with complex interactions [16]. Application of such method leads to an improvement in reaction yields and to a better prediction of output response to nominal and target requirements in least time with low cost procedure [17, 18]. In the present study, a novel adsorbent (Ruthenium nanoparticles loaded on activated carbon (Ru-NPs-AC)) was synthesized by applying ultrasound in simple manner. This adsorbent was then applied for the simultaneous removal of Methylene blue (MB) and Pb^{2+} ions. The effects of variables such as initial dye and Pb^{2+} ion concentrations (mg L^{-1}), adsorbent doses (g) and contact time (min) on the simultaneous removal of MB and Pb^{2+} ions were studied. The possible interaction

between the parameters was studied. Optimization was performed using central composite design (CCD) under response surface methodology [19].

2. Experimental

2.1 Material and instrument

Chemicals including NaOH, HCl, and nitrate salt of Pb^{2+} ions with the highest purity available were purchased from Merck (Darmstadt, Germany). Methylene blue (MB) was purchased from (Sigma–Aldrich). The chemical information of MB dye are (a) color index number: 52.015, (b) molecular weight: 319.86 g/mol, (c) empirical formula: $C_{16}H_{18}N_3SCl$ and (d) λ_{max}: 664 nm. Both target species solution was prepared in double distilled water and subsequently, their standard solution (100 mg L^{-1}) was used as working solution for following adsorption experiments. The pH was adjusted and measured using pH/Ion meter Metrohm, model 692. The MB spectra were recorded over 300 nm to 750 nm by using Jasco UV-Visible spectrophotometer, model V-530 with a fixed slit width of 2 nm and scan speed of 1000 nm/min. Pb^{2+} ions were determined using an atomic absorption spectrophotometer (Varian, model AA240). Fourier transform infrared spectroscopy (FTIR) absorption spectra were obtained using KBr discs by a FTIR 6300 in the region 400–4000cm^{-1}. X-ray diffraction (XRD) pattern was recorded by an automated Philips X'Pert X-ray diffractometer using Cu Kα radiation (40 kV and 30 mA) for 2θ values over 30 - 100º following the separation of Ruthenium nanoparticles (Ru NPs) from the aqueous suspension by the centrifugation at 4000 rpm and drying Ru NPs. The shape and surface morphology of the Ru NPs were investigated by field emission scanning electron microscope (FESEM, Hitachi S4160) under an acceleration voltage of 15 kV.

2.2 preparation of Ru-NPs-AC

Ruthenium nanoparticles (Ru NPs) were synthesized based on the reaction of the mixture of Ruthenium chloride ($RuCl_3$) with ascorbic acid in ethylene glycol. Briefly, Poly (N-vinyl-2-pyrrolidone) (PVP) and $RuCl_3$ solution (2×10^{-3} M) with 8:1 mole ratio were thoroughly mixed and dissolved in ethylene glycol under ultrasound irradiation. Then, 2 mL of ascorbic acid (0.1 M) was separately added to the above solution. The mixture was exposed to ultrasound radiation at 60 °C for different times in the range of 10-50 min. The formation of Ru nanoparticles was evident from the change in solution color from yellow to dark brown after 30 min. In the next step, 100 mL of the freshly prepared Ru-NPs solution (6.8×10^{-2} mg L^{-1}) was mixed with AC (5.0 g) in a 250 mL Erlenmeyer flask under ultrasound radiation for 12 h. After the deposition of Ru-NPs onto

AC, the Ru-NP-AC mixture was filtered and washed several times using deionized water. Then, it was dried at 110 °C in an oven for 10 h.

2.3 Multi-component adsorption of MB dye and Pb^{2+} ions onto Ru-NPs-AC

The competitive and simultaneous adsorption of MB and Pb^{2+} ions onto Ru-NPs-AC were studied. All experiments were carried out at room temperature at various conditions, according the designed experiments, in 100 mL beaker on a magnetic stirrer (300 rpm) to find the optimum initial dye and Pb^{2+} ions concentration, adsorbent dosage and contact time. The effect of pH on whole protocol (40 mg L^{-1} of Pb^{2+} ions and 40 mg L^{-1} of MB mixed with 0.02 g of adsorbent over pH range of 2 - 7) was investigated and experiments was conducted until reaching equilibrium. After pH optimization, CCD experiments were followed to investigate and evaluate the effect of individual variables as well as their possible interactions on the removal percentage of MB dye and Pb^{2+} ions as responses. Design Expert 7 software was used for the statistical analysis of results obtained from the experimental design. The kinetic studies are important to identify the equilibrium time, and the calculation of adsorption rates are useful for process design for understanding the possible adsorption mechanisms. The kinetic adsorption parameters were determined using binary solutions at optimum concentration of adsorbent. For isotherm studies, single and binary solutions with various concentrations of MB dye and Pb^{2+} ion above and below the optimal point were investigated with 0.018 g of adsorbent. Concentrations of each species in single and binary system were studied and there was a constant ratio between the concentrations of the two species.

Optimum pH, which was approximately around natural value of the multi-component solutions (5 to 6), was used for the evaluation of kinetic and equilibrium data. The results of mono- and multi- component investigation were obtained and compared at previously optimized conditions. The capacities for the adsorption of heavy metal ions and dye (q_i, mg/g) onto the adsorbent were calculated by:

$$q_i = \frac{(C_{0,i} - C_{f,i})V}{m}, \qquad (1)$$

where $C_{0,i}$ and $C_{f,i}$ are the initial and final concentration (mgL^{-1}) of pollutant *i* (i.e., dye or heavy metal ion) in the binary solution, *V* is the volume (L) of dye – metal ion solution used for the adsorption experiments, and m is the mass (g) of adsorbent.

2.4 Experimental design

Central composite design (CCD) which is the most popular response surface method (RSM) design was applied to design a series of experiments with least number of experiments. This approach helps us to investigate the effect of parameters involved (i.e. the concentration of MB, the concentration of Pb^{2+}, adsorbent amount and contact time) on the responses (i.e. the removal percentages MB and Pb^{2+}) in a cost- and time- effective way. It also helps consuming less amount of material to be environmental friendly. The CCD under RSM makes it feasible to observe the possible interaction of the parameters and their influences on the responses. Numeric factors (four factors) were varied over five levels including two levels for star or axial points (+/–α), two levels for factorial points or high/low levels (+/–1) and one level for center point (See Table 1). Seven replicates were made for center point and 24 for not centers, which made a CCD with overall 31 experimental runs (See Table 2). Note that the CCD alpha value is the distance that the star points are from the center of the design space. Alpha for the CCD in this work was calculated to be 2 according $\alpha = 2^{k/4}$, where k is the number of factors (= 4). The complete quadratic model for this 4-factor CCD is given by

$$Y = b_0 + \sum_{i=1}^{4} b_i x_i + \sum_{i=1}^{4} b_{ii} x_i^2 + \sum_{i=1}^{4} \sum_{j=i+1}^{4} b_{ij} x_i x_j , \qquad (2)$$

where Y is the predicted response (removal percentage of either MB dye or Pb^{2+} ion: R%); x_i's are the independent variables that are known for each experimental run. The parameter b_0 is the model constant; b_i's are the linear coefficients; b_{ii}'s are the quadratic coefficients and b_{ij}'s are the interaction coefficients.

3. Results and discussion

3.1 Characterization of adsorbent

Bubbles generated by ultrasound and their implosive collapse in a liquid make the chemical reactions facile and fast. An ultra-sonication was applied for the synthesis of Ruthenium nanoparticles. Spherical Ru-NPs achieved in the presence of ultrasound irradiation (30 W/cm^2 applied at various times) significantly increased in mass and homogeneous nature. Diameters of the particles produced at various sonication conditions were less than 200 nm, while higher time led to the production of nonhomogeneous particles. After 30 min (optimum time) ultra-sonication, nanoparticles with size smaller than 80 nm were obtained according to SEM image. In addition, the position and intensity of Ru-NP surface Plasmon resonance were used as a good criterion for estimating the size and shape of nanoparticles. An increase in the number of nanoparticles and a decrease in their size were observed with increasing the sonication time up to 30 min. This was seen as a decrease in the intensity of absorbance spectra with a blue shift in maximum wavelength. The larger size achieved at shorter

sonication time, was probably due to agglomeration and coagulation where the nanoparticles found to be monodisperse. The Ostwald ripening growth mechanism can simply explain this behavior [20]. As mentioned above, ultrasound induces chemical or physical changes during cavitations that generate hot local regions (around 5000 °C) and high pressures (about 500 atm) in reasonable time (few microseconds) that accelerate the rate of reactions and make the ultrasonic-assisted synthesis of nanoparticles as a simple, low cost, effi2cient and environmental-friendly approach through homogeneous nucleation and a substantial reduction in crystallization time [14,21].

Fig. 1 shows the UV-Vis absorption spectra obtained at different time of ultra-sonication exposed to reaction mixture under reflux (ascorbic acid, $RuCl_3$ in ethylene glycol at 160 ºC). The yellow solution before reflux until 10 min shows a peak around 405 nm that is attributed to ligand to metal charge transfer (after immediate mixing and application of heating and ultrasound to the mixture) [16]. Strong decrease in the intensity of this peak with time after 30 min strongly confirms the efficient reduction of Ru^{3+} ions to Ru^0. This behavior is coinciding with color change from yellow into dark brown and with absorbance spectrum red shift from ultraviolet to visible region attributed to the formation of the Ru nanoparticles.

X-ray diffraction (XRD) pattern of Ru NPs powder (Fig. 2) are well supported by reference XRD pattern for Ru (Joint Committee for Powder Diffraction Standards, JCPDS card No. 04-0836) confirming the face centered cubic (fcc) crystal structure of Ru-NPs. The average nanocrystallites size (D) is estimated according to the Debye–Scherer Equation [22]:

$$D = \frac{K\lambda}{\beta \cos\theta} \qquad (3)$$

where K is a correction factor having value 0.9, λ is the X-ray wavelength (1.5405 °A), β is the full width at half maximum (FWHM) of diffraction peak in radians and θ is the Bragg's angle. Based on the full width at half maximum of the most intense peak (111), the average size of Ru NPs was estimated to be about 23 nm.

The FESEM images of the AC and Ru-NP-AC are shown in Fig. 3. The figure shows homogeneous, highly porous, relatively smooth Ru-NPs with diameters in the range of 20-50 nm. The particle size measured directly from FESEM image is consistent to the XRD analysis.

The EDS mapping of the Ru-NP-AC was shown in Fig. 4 in order to investigate their localized elemental information. It is worth noting that the element of Ru was well dispersed on the surface of AC.

The BET surface area of AC and Ru-NPs loaded on AC was measured and shown in Table 3. A high surface area (1266 m^2/g) of Ru-NP-AC makes it suitable as a very good adsorbent.

3.2 Effect of pH on removal efficiency

Fig. 5 presents the variation of MB and Pb^{2+} ions removal by using Ru-NPs-AC at varying solution pH. It was expected that both target compounds can strongly be adsorbed onto the sorbent at neutral or close to alkaline pH. The increase in pH can significantly enhance the removal percentage of Pb^{2+} only, while the removal of MB was not significantly affected. It is because of the fact that adsorbent becomes positively charged at low pHs due to the protonation of AC functional groups. This significantly increases the repulsion force between positively charged AC and Pb^{+2} causing less adsorption. Raising the pH near to neutral value (7), makes the formation of reactive centers (following dissociation of AC functional groups) possible that leads to an enhancement in adsorption rate and magnitude. It seems that this zero valiant nanoparticle has distinguished surface Plasmon resonance peaks that make it possible for more attraction of organic species such as MB. Therefore, a higher removal percentage of MB than that of Pb^{2+} ions is expected. At pH above 7, increase in adsorption percentage is ascribed to the surface attraction and accumulation of each species as sole particles or following their complexation. As mentioned above, the effect of pH in case of MB is lower than Pb^{2+} ions. It is well known that heavy metal ions react with hydroxyl species in basic solution. For MB, as a basic dye, it forms cation (C^{+}) and reduced ions (CNH^{+}) in solution. As the pH of the dye solution becomes higher, the association of cationic dyes on solid will take place more easily and makes significant enhancement in its removal percentage [23, 24]. After investigating the pH effect, the work continuation was performed in natural pH of solution over the range of 5.2 to 5.7. The pHpzc value (the pH at the point of zero charge) of the adsorbent understudy was found to be 5.4 ± 0.4. At pH less than pHpzc, sorbent surface has positive charge following the adsorption of H^{+} ions onto AC functional group including hydroxyl or carboxylic groups. Therefore, a repulsive force occurs between the metal ions and the sorbent surface, which causes a decrease in the recoveries. At higher pH value (pH>6), the probable formation of insoluble M(OH)n or $M(OH)^{+}$ as competitive reaction hinders the transfer and diffusion of Pb^{2+} ions to the external adsorbent surface. After the pH optimization, removal efficiency of dye improved from 77% to 99% for the condition mentioned in Table 2.

3.3. Optimization approach

The removal percentages of MB and Pb^{2+} ions were statistically studied as a function of the MB concentration (x_1), Pb^{2+} ions concentration (x_2), amount of adsorbent (x_3) and contact time (x_4). These four factors and their levels are shown in Table 1. The experimentally recorded responses values are tabulated in

Table 2. At first, without any data transformation, a model according Eq. (4) was applied for each response and then the analysis of variance (ANOVA) was performed. For instance, this full model for the removal percentage of MB ($R\%_{MB}$) showed a good model F value (13.02) and P value (0.0001) with a lack of fit P value of 0.1125 all confirming that the model well applies for correlating the $R\%_{MB}$ to the four factors involved. However, the P values corresponding the terms x_1, x_2, x_3, x_4, x_1x_3 and x_3^2 are less than 0.05 and thus they are significant model terms, which should only be included in the model to obtain an even better improved model. As seen, in addition to the linear terms of x_1, x_2, x_3 and x_4, the interaction term of x_1x_3 as the interaction of the MB concentration and the amount of adsorbent as well as the quadratic term of x_3^2 influence the $R\%_{MB}$. Therefore, the following Response Surface Reduced Quadratic Model was finally applied for $R\%_{MB}$.

$$R\%_{MB} = +96.1513 - 0.9437\,x_1 - 0.0984\,x_2 + 1729.3596\,x_3 + 0.1015\,x_4 + 41.8000\,x_1x_3 - 72350.8772\,x_3^2 \quad (4)$$

The ANOVA was performed for this reduced model for $R\%_{MB}$ (See Table 4) and showed a larger lack of fit P value (0.1755) confirming the better applicability of the reduced model than the full one for $R\%_{MB}$.

A similar procedure was followed to model the removal percentage of Pb^{2+} ($R\%_{Pb^{2+}}$). A final model which applies well for $R\%_{Pb^{2+}}$ was found to be as follows:

$$R\%_{Pb^{2+}} = +56.3799 - 0.62987\,x_1 - 0.6007\,x_2 + 965.9167\,x_3 + 0.1506\,x_4 + 20.5250\,x_1x_3 \quad (5)$$

The ANOVA for this model for $R\%_{Pb^{2+}}$ (See Table 5) showed a model F value of 131.76 and a lack of fit P value of 0.1805 (larger than 0.05) confirming the well applicability of the model. As seen in Eq. (5), the linear terms of x_1, x_2, x_3 and x_4 are significant model terms in addition to the interaction term of x_1x_3.

From these predictive models, it is needed to find the best condition at which the responses are maximized. It was found to be 30 mg L^{-1}, 22.65 mg L^{-1}, 0.018 g and 27 min for the concentration of MB, concentration of Pb^{2+}, adsorbent dosage and contact time, respectively. At this condition, the $R\%_{MB}$ and $R\%_{Pb^{2+}}$ were found to be 98.96 % and 56.59 %, respectively with composite desirability of 0.95 which is very close to 1. To make a test on the validity of the prediction of the model, the experiment corresponding to the optimum condition was run for three times and average removal percentages of 99.97% and 55.94 % were obtained for MB and Pb^{2+} ions,

respectively which is in high agreement with the predicted values. A 3D plot of $R\%_{MB}$ vs. the concentration of Pb^{2+} ion and the adsorbent dosage is shown in Fig. 6, while the concentration of MB and contact time were kept at their optimum values i.e. 30 mgL^{-1} and 27 min, respectively.

3.4. Kinetic study

It is important to predict the removal rate of pollutants from aqueous solutions [25]. Experimental results indicated that the adsorbed amount of MB and Pb^{2+} ions increased with increasing contact time and reaches equilibrium after around 25 min. Different kinetic models including pseudo-first order, pseudo-second order, intraparticle diffusion and Elovich model were applied to investigate the mechanism of adsorption and potential rate controlling steps such as chemical reaction, diffusion control and mass transport processes. The kinetic adsorption parameters were determined using binary solutions at optimum concentration of adsorbent (0.018 g). The pseudo-first order, pseudo-second order, intraparticle diffusion and Elovich model equations are shown in Table 6 [26]. q_e (mg/g) and q_t (mg/g) are defined to be the adsorption capacities at equilibrium and at time t (min), respectively. K_1 is defined to be the pseudo first-order rate constant (1/min). In pseudo-second order rate equation, K_2 is the order rate constant (g/(mg min)). In addition, the initial adsorption rate, h (mg/(g min)) can be determined from K_2 and q_e values using the following relation:

$$h = K_2 q_e^2 \qquad (6)$$

K_{diff} is the intraparticle diffusion rate constant (mg/(g $min^{1/2}$)) and C is a representative for boundary layer resistance and thickness. If the adsorption kinetic fits the Elovich model, a plot of q_t vs. $ln(t)$ should yield a linear relationship with a slope of $(1/\beta)$ and an intercept of $(1/\beta)\ ln(\alpha\beta)$. All the kinetics constants values are determined and shown in Table 6. The pseudo-first order constants (q_e, K_1 and R^2) for MB and Pb^{2+} adsorption onto Ru-NPs-AC were also presented in Table 6. The theoretical q_e values calculated from the first-order kinetic model did not agree with the experimental values, and the correlation coefficients were also found to be slightly lower. These results indicated that the pseudo-first order kinetic model is not appropriate for modeling the adsorption of MB and Pb^{2+} ions onto Ru-NPs-AC.

The slope and intercept of the linear plot t/q_t versus t are used for the evaluation of the values of q_e and K_2 (Table 6). The obtained R^2 values were higher than 0.99 and the theoretical q_e values were very close to the experimental q_{exp} values. Thus, the adsorption of MB and Pb^{2+} ions on Ru-NPs-AC was well described by the pseudo-second order kinetic model strongly supporting that the adsorption of both species follows chemisorption through the sharing or exchange of electrons between adsorbent and pollutants. The h and K_2

values calculated from the pseudo-second-order kinetic model were higher for MB than Pb^{2+}, indicating that the adsorption of MB onto Ru-NPs-AC was much faster than that of Pb^{2+} ion. The value of R^2 for Elovich model is low. Therefore, this model is not appropriate to describe the present adsorption behavior.

3.5 Isotherm study

Adsorption equilibrium isotherm is designed based on mathematical relation of the amount of adsorbed target per gram of adsorbent (q_e (mg/g)) to the equilibrium non-adsorbed amount of adsorbate in the solution (C_e (mg/L)) at fixed temperature [27]. This analysis has been used to study and characterize the performance of Ru-NPs-AC in the removal of MB and Pb^{2+} ions under competitive conditions. For isotherm studies, single and binary solutions with various concentrations of dye (25, 30 and 35 mg L^{-1}) and metal ion (17.5, 22.5 and 27.5 mg L^{-1}) which are around the optimal points were investigated with 0.018 g of adsorbent.

The Langmuir model as mostly applied model is presented below [28]:

$$q_e = \frac{Q_m K_L C_e}{1 + K_L C_e}, \quad (7)$$

where C_e, Q_m and K_L are the concentration of adsorbate at equilibrium (mgL^{-1}), maximum mono layer adsorption capacity (mg g^{-1}) and Langmuir constant (L mg^{-1}), respectively. These parameters were simply calculated by plotting C_e/q_e vs. C_e. The slope and intercept of C_e/q_e vs C_e line are used to estimate the value of above-mentioned parameters. The essential characteristics of the Langmuir isotherm can be expressed by a dimensionless constant (R_L) which is generally defined by the following equation [29, 30]:

$$R_L = \frac{1}{1 + K_L C_0}, \quad (8)$$

where, C_0 is the initial concentration (mg/L). The nature of the adsorption process might be either unfavorable (R_L>1), favorable ($0<R_L \leq 1$) or irreversible (R_L=0). For both species, the R_L value was lower than 1 supporting the favorable nature of adsorption process. The values of Q_m, K_L, R_L and the correlation coefficient (R^2) are shown in Table 7.

To perform data analysis, the effect of both dye and heavy metal in multi-component removal performance of Ru-NPs-AC has been studied and determined using the P-factor. This method is a correlative technique that has been developed and applied to multi component systems [29]. It is an easy-to-use method based on a ‘‘lumped’’ capacity factor p_i.

$$p_i = \frac{(Q_{m,i})_{\text{single solute}}}{(Q_{m,i})_{\text{multi solute}}}, \qquad (9)$$

where $(Q_{m,i})_{\text{single solute}}$ is the maximum monolayer adsorption capacity for pollutant *i* in the single solution, and $(Q_{m,i})_{\text{multi solute}}$ is the maximum monolayer adsorption capacity of that pollutant with the same initial concentration in a multi-component solution. Literature indicates that: (a) if $p_i > 1$, the adsorption of pollutant *i* is promoted by the presence of other pollutants, (b) if $p_i = 1$, there is no effect on adsorption capacity of pollutant *i*, and (c) if $p_i < 1$, the presence of other pollutants suppresses the adsorption of pollutant [31-33].

The results show that the increment of each pollutant concentration significantly affects the uptake of the other in the bi-pollutant system. It is to be noted that the adsorption capacities for Pb^{2+} ions can be decreased (i.e., $p_i >$ 1.0) by the presence of MB in binary solutions and also decrease in uptake of MB in binary solution. This decrease is lower compared to Pb^{2+} ions because of the lower value of P_{MB} toward $P_{Pb^{2+}}$ (see Table 7).

Freundlich isotherm can be expressed by [34]:

$$q_e = K_F C^{1/n}, \qquad (10)$$

where, K_F is adsorption capacity at unit concentration and 1/n is adsorption intensity. 1/n values indicate the type of isotherm to be irreversible (1/n=0), favorable (0<1/n<1), unfavorable (1/n>1). Eq. (11) can be modified to a linear form:

$$\log q_e = \log K_F + (1/n) \log C_e \qquad (11)$$

Linear form of log q_e versus log C_e was plotted and the values of K_F, 1/n and correlation coefficient (R^2) of single and binary system were calculated (Table 7). The linear form of Tempkin isotherm is given as:

$$q_e = B_1 \ln K_T + B_1 \ln C_e \qquad (12)$$

where, $B_1 = \frac{RT}{b}$ is related to the heat of adsorption, T is the absolute temperature in Kelvin and R (8.314 J mol^{-1} K^{-1}) is the universal gas constant [41]. A plot of q_e versus $\ln C_e$ enables the determination of the isotherm constants B_1 and K_T from the slope and the intercept, respectively. K_T is the equilibrium binding constant (L mol^{-1}) corresponding to the maximum binding energy and constant B_1 is related to the heat of adsorption. The values of K_T, B_1 and R^2 (correlation coefficient) are shown in Table 7.

The Dubinin–Radushkevich (D–R) isotherm model was applied to estimate the porosity, free energy and the characteristics of adsorbents [42]. The D–R isotherm is applicable to homogeneous surfaces. Constant adsorption potential is calculated from the following linear equation.

$$\ln q_e = \ln Q_s - B\varepsilon^2, \quad (13)$$

where B is a constant related to the adsorption energy, Q_s is the theoretical saturation capacity and ε is the Polanyi potential which is generally calculated from Eq. (14).

$$\varepsilon = RT \ln(1 + 1/C_e). \quad (14)$$

The slope of the plot of $\ln q_e$ versus ε^2 gives B ($mol^2/(kJ^2)$) and the intercept yields the adsorption capacity, (Q_s (mg/g)). The calculated values of D–R parameters in single and binary systems are shown in Table 7. The correlation coefficient value (R^2) for Langmuir isotherm is close to 1 (0.99) which dictates that both MB and Pb^{2+} adsorption on Ru-NPs-AC follow Langmuir isotherm model better than the Freundlich, Temkin and D-R isotherms.

4. Conclusion

Ru-NPs-AC was prepared as adsorbent with effective surface area of 1266 m^2/g. The prepared adsorbent was used for the simultaneous removal of MB and Pb^{2+} ion from their aqueous mixture. The effective parameters were optimized by central composite design. The optimum adsorbent mass was found to be 18 mg for 30 mg L^{-1} of MB and 22.65 mg L^{-1} of Pb^{2+} ions in 27 min. The maximum removal percentage was found as about 99% for MB and 56% for Pb^{2+} in short time (<27 min). The adsorption follows pseudo second order kinetic model. The equilibrium adsorption data were better represented by Langmuir isotherm model. The maximum adsorption capacity was 41.6 mg/L and 19.3 mg/L of MB and Pb^{+2}, respectively from their mixture. It is inferred that the Ru-NPs-AC may be used as effective adsorbent in alternate to commercial activated carbon for the removal of MB and Pb^{+2} from waste water. However, further investigation on scale up, mechanism involved and techno economic aspect is to be explored.

References

1. M. Ghaedi, S. Hajjati, Z. Mahmudi, I. Tyagi, Shilpi Agarwal, A. Maity, and V. K. Gupta. Chem. Eng. J. 2015, **268,** 28-37.
2. S. Chakravarty, Ashok Mohanty, T. Nag Sudha, A.K. Upadhyay, J. Konar, J.K. Sircar, A. Madhukar, K.K. Gupta, J. Hazard. Mater 2010, **173,** 502–509
3. M. Visa, C. Bogatu, A. Duta, Appl. Surf. Sci. 2010,**256**, 5486–5491.
4. S. Zhang, J. Li, M. Zeng, J. Li, J. Xu, and X. Wang. Chem.-A Europ. J. 2014, **20**, 9805-9812.
5. S. Zhang, Meiyi Zeng, Jiaxing Li, Jie Li, Jinzhang Xu, and Xiangke Wang. J. Mater. Chem. A. 2014, **2**, 4391-4397.
6. S. Zhang, J. Li, X. Wang, Y. Huang, M. Zeng and J. Xu. Jo. Mater. Chem. A. 2015, **3** 10119-10126.
7. S. Zhang, W. Xu, M. Zeng, J. Li, J. Li, J. Xu and X. Wang. J. Mater. Chem. A. 2013, **1** 11691-11697.
8. S. Zhang, J. Li, X. Wang, Y. Huang, M. Zeng and J. Xu. ACS appl. Mater. Interfaces. 2014, **6,** 22116-22125.
9. M. Ghaedi, B. Sadeghian, A. Amiri Pebdani, R. Sahraei, A. Daneshfar, C. Duran, Chem. Eng. J. 2012, **187**,133– 141.
10. S. Kuriakose, B. Satpati, and S. Mohapatra. Phys. Chem. Chem. Phys. 2014, **16**, 12741-12749.
11. S. Kuriakose, V. Choudhary, B. Satpati, and S. Mohapatra. Beilstein j. Nanotechnol. 2014, **5**, 639-650.
12. S. Kuriakose, V.Choudhary, B. Satpati, and S. Mohapatra. Phys. Chem. Chem. Phys. 2014, **16,** 17560-17568.
13. S. Kuriakose, N. Bhardwaj, J. Singh, B. Satpati, and S. Mohapatra Beilstein j. nanotechnol. 2013, **4**, 763-770.
14. S. Hajati, M. Ghaedi, B. Barazesh, F. Karimi, R. Sahraei, A. Daneshfar, A. Asghari, J. Ind. Eng. Chem., 2014, **20,** 2421-2427.
15. M. Ghaedi, M. Pakniat, Z. Mahmoudi, S. Hajati, R. Sahraei, A. Daneshfar, Spectrochim. Acta A, 2014, **123**, 402-409.
16. M. Ghaedi, H. Mazaheri, S. Khodadoust, S. Hajati, M.K. Purkait, Spectrochim. Acta Part A. 2015**, 135**, 479–490.
17. Ghaedi, M., S. Hajati, M. Zare, M. Zare, and S. Y. Shajaripour Jaberi. RSC Adv. 2015, **5,** 38939-38947.
18. A. Asfaram, M. Ghaedi, S. Agarwal, I. Tyagi, and V. K. Gupta. RSC Adv. 2015, **5**, 18438-18450.
19. S. Hajati, M. Ghaedi, F. Karimi, B. Barazesh, R. Sahraei, A. Daneshfar, J. Ind. Eng. Chem., 2014, **20**, 564-571.
20. N.M. Mahmoodi, R. Salehi, M. Arami, Desalination, 2011, **272,** 187–195
21. X. Li, Y. Li, Sidi Zhanga, Zhengfang Yeb, Chem. Eng. J. 2012 **183**, 88– 97
22. N. Dehghanian, M. Ghaedi, A. Ansari, A. Ghaedi, A. Vafaei, M. Asif, S. Agarwal, I. Tyagi, and V. K. Gupta. *Desalinat. Water Treat.* 2015 1-14.
23. A. Asfaram, M. Ghaedi, A. Goudarzi and M. Soylak. *RSC Adv.* 2015, **5,** 39084-39096.
24. M. Ghaedi, A. Asfaram, B. Mirtamizdoust, A. A. Bazrafshan and S. Hajati. *RSC Adv.* 2015, **5**, 42376-42387.
25. Ghaedi, Mehrorang, Z. Rozkhoosh, A. Asfaram, B. Mirtamizdoust, Z. Mahmoudi, and A. A. Bazrafshan, *Spectrochim. Acta Part A,* 2015, **138,** 176-186.
26. Hajati, S., M. Ghaedi, and S. Yaghoubi. *J. Ind. Eng. Chem.* 2015, **21,** 760-767.
27. Ghaedi, M., N. Zeinali, M. Maghsoudi, and M. K. Purkait. *J. Disper. Sci. Technol.* 2015, **36**, 1339-1348.
28. I. Langmuir, J. Am. Chem. Soc. 1916, **38**, 2221–2295.
29. S.K. Das, J. Bhowal, A.R. Das, A.K. Guha, Langmuir 2006, **22**, 7265–7272.
30 M. Ghaedi, S. Hajati, B. Barazesh, F. Karimi, G. Ghezelbash, J. Ind. and Eng. Che. 2013, **19**, 227–233
31. C.A. Basar, J. Hazard. Mater. 2006, **135**, 232–241.
32. S. Senthilkumaar, P. Kalaamani, K. Porkodi, P.R. Varadarajan, C.V. Subburaam, Bioresour. Technol. 2006, **97,** 1618–1625.
33. W.J. Weber, J.C. Morris, J. Sanit. Eng. Div. Am. Soc. Civ. Eng. 1963, **89**, 31–60.
34. Freundlich, H.M.F., Zeitschrift fur Phys. Chem. 1906, **57**, 385–470.
35. M. Ghaedi, A. Ansari, M. H. Habibi, and A. R. Asghari. *J. Ind. Eng. Chem.* 2014, **20**, 17-28.
36. Ghaedi, M., A. M. Ghaedi, M. Hossainpour, A. Ansari, M. H. Habibi, and A. R. Asghari. *J. Ind. Eng. Chem.* 2014, **20**, 1641-1649.

Figure captions:

Fig. 1: Temporal evolution of UV-Vis absorption spectra of the Ru nanoparticles

Fig. 2: X-ray diffraction (XRD) pattern of the Ru nanoparticles

Fig. 3: FESEM images of (a) the activated carbon (taken from Ref. 14) (b) the Ru-NP-AC

Fig. 4: FESEM image and the EDS mapping Ru and C.

Fig. 5: Effect of pH on removal percentage of MB and Pb^{2+} in multi solute system

Fig. 6: 3D plot of $R\%_{MB}$ vs. the concentration of Pb^{2+} ion and the adsorbent dosage while the concentration of MB and contact time were kept at their optimum values i.e. 30 mgL^{-1} and 27 min, respectively.

Tables caption:

Table 1: Factors and levels in the CCD.

Table 2: CCD experiments and the responses obtained.

Table 3: Information obtained by BET taken from AC and Ru-NP-AC.

Table 4: ANOVA for the model applied for the MB removal percentage.

Table 5: ANOVA for the model applied for the Pb^{2+} removal percentage.

Table 6: Kinetic parameters for the simultaneous removal of MB and Pb^{2+} from multi-component system.

Table 7: Parameters of different Isotherms for Ru-NPs-AC multi-component system.

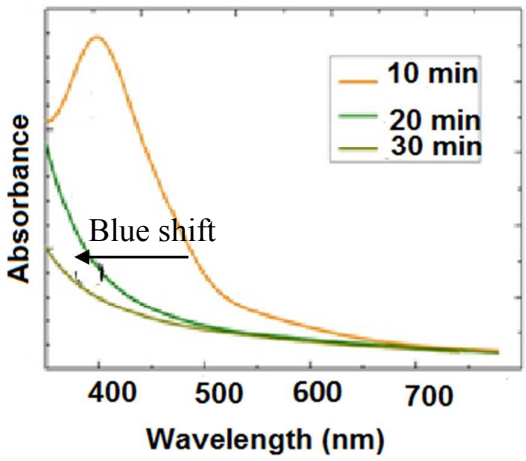

Fig. 1

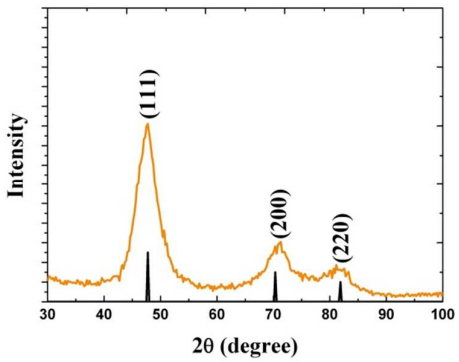

Fig. 2

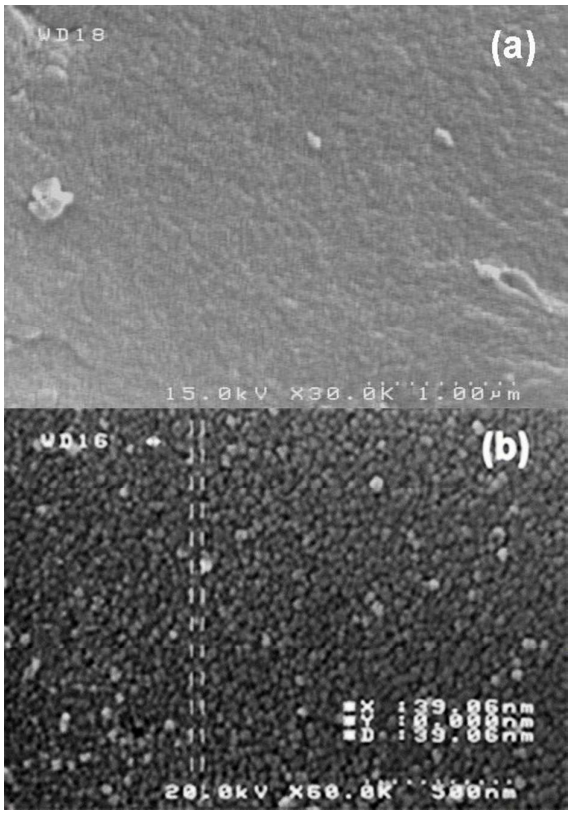

Fig. 3

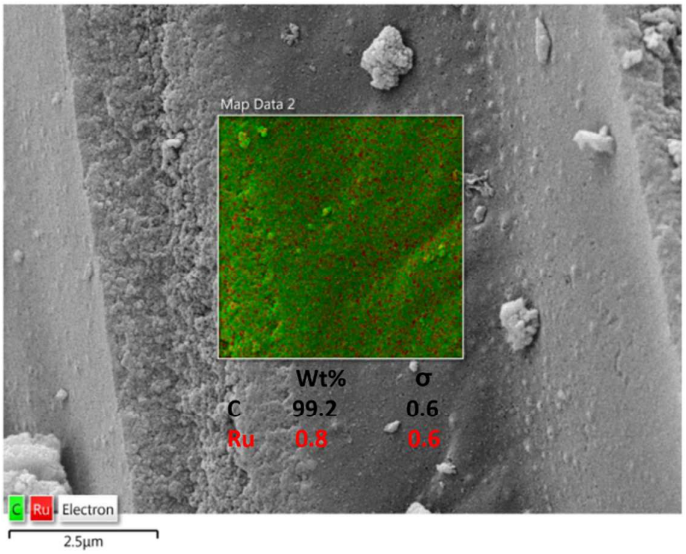

Fig. 4

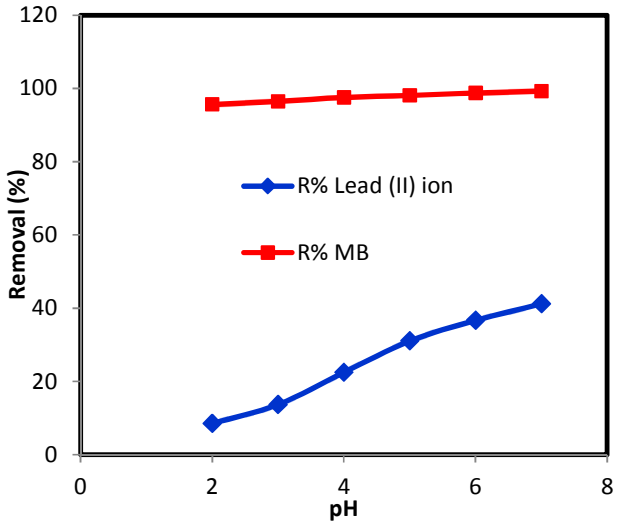

Fig. 5

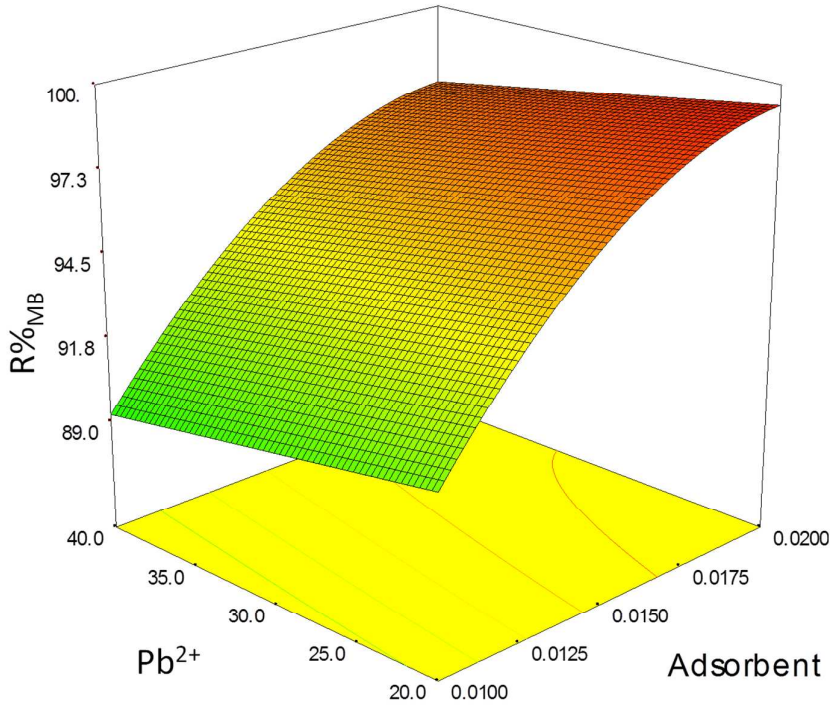

Fig. 6

Table 1: Factors and levels in the CCD

Factors	levels			(α=2)	
	Low (−1)	center (0)	high (+1)	−α	α+
x_1 (MB concentration (mg L^{-1}))	20	30	40	10	50
x_2 (Pb^{2+}concentration (mg L^{-1}))	20	30	40	10	50
x_3 (adsorbent mass (g))	0.010	0.015	0.020	0.005	0.025
x_4 (time (min))	17.5	30	42.5	5	55

Table 2: CCD experiments and the responses obtained

Run	x_1	x_2	x_3	x_4	R% MB	R% Pb^{2+}
1	30	30	0.015	30	94.12	47.22
2	30	30	0.015	30	97.02	48.76
3	30	30	0.015	30	98.82	49.48
4	30	30	0.015	30	96.58	47.92
5	30	30	0.015	30	95.12	46.38
6	30	30	0.015	30	97.27	45.94
7	30	30	0.015	30	96.15	49.79
8	30	30	0.025	30	99.95	65.21
9	30	30	0.005	30	76.69	32.5
10	30	30	0.015	55	99.01	54.13
11	30	30	0.015	5	89.58	42.19
12	50	30	0.015	30	88.62	42.51
13	30	50	0.015	30	96.81	38.54
14	10	30	0.015	30	99.91	55.72
15	30	10	0.015	30	99.15	64.28
16	20	20	0.01	17.5	97.25	48.04
17	20	20	0.02	17.5	99.81	59.72
18	20	20	0.01	42.5	99.03	52.74
19	20	20	0.02	42.5	99.93	64.97
20	20	40	0.01	17.5	95.31	34.67
21	20	40	0.02	17.5	98.95	49.5
22	20	40	0.01	42.5	97.45	37.34
23	20	40	0.02	42.5	99.14	52.58
24	40	20	0.01	17.5	87.18	38.42
25	40	20	0.02	17.5	98.19	56.74
26	40	20	0.01	42.5	89.12	40.65
27	40	20	0.02	42.5	99.12	59.2
28	40	40	0.01	17.5	83.53	29.97
29	40	40	0.02	17.5	94.15	46.42
30	40	40	0.01	42.5	85.78	30.11
31	40	40	0.02	42.5	96.38	47.19

Table 3: Information obtained by BET taken from Ru nanoparticles on activated carbon.

Summary Report	AC	Ru-NP-AC
BET Surface Area	209.7389 m^2/g	1266.0221 m^2/g
Langmuir Surface Area	297.8578 m^2/g	1734.0809 m^2/g
BJH Adsorption cumulative surface area of pores between 17.000 Å and 3000.000 Å width**:**	240.695 m^2/g	111.157 m^2/g
BJH Desorption cumulative surface area of pores between 17.000 Å and 3000.000 Å width	301.1900 m^2/g	125.2192 m^2/g
BJH Adsorption cumulative volume of pores between 17.000 Å and 3000.000 Å width**:**	0.404031 cm^3/g	0.103866 cm^3/g
BJH Desorption cumulative volume of pores between 17.000 Å and 3000.000 Å width:	0.402143 cm^3/g	0.109881 cm^3/g
t-Plot micropore volume	-0.016885 cm^3/g	0.214044 cm^3/g
Adsorption average pore width (4V/A by BET)	74.6003 Å	19.8342 Å
BJH Adsorption average pore width (4V/A)	67.144 Å	37.376 Å
BJH Desorption average pore width (4V/A)	53.407 Å	35.101 Å

Table 4: ANOVA for the model applied for the MB removal percentage.

Source	Sum of Squares	Degree of Freedom	Mean Square	F value	P value Prob > F
Model	865.08	6	144.18	33.42	< 0.0001
x_1 (MB concentration)	240.67	1	240.67	55.79	< 0.0001
x_2 (Pb^{2+}concentration)	23.25	1	23.25	5.39	0.0291
x_3 (adsorbent dosage)	396.42	1	396.42	91.89	< 0.0001
x_4 (contact time)	38.61	1	38.61	8.95	0.0063
$x_1 x_3$	69.89	1	69.89	16.20	0.0005
x_3^2	96.25	1	96.25	22.31	< 0.0001
Residual	103.54	24	4.31		
Lack of Fit	89.62	18	4.98	2.15	0.1755
Pure Error	13.92	6	2.32		
Cor Total	968.62	30			

Table 5: ANOVA for the model applied for the Pb^{2+} removal percentage.

Source	Sum of Squares	Degree of Freedom	Mean Square	F value	P value Prob > F
Model	2717.91	5	543.58	131.76	< 0.0001
x_1 (MB concentration)	248.84	1	248.8	60.32	< 0.0001
x_2 (Pb^{2+}concentration)	866.16	1	866.16	209.94	< 0.0001
x_3 (adsorbent dosage)	1501.00	1	1501.00	363.82	< 0.0001
x_4 (contact time)	85.05	1	85.05	20.62	0.0001
$x_1 x_3$	16.85	1	16.85	4.08	0.0541
Residual	103.14	25	4.13		
Lack of Fit	89.72	19	4.72	2.11	0.1805
Pure Error	13.42	6	2.24		
Cor Total	2821.05	30			

Table 6: Kinetic parameters for the simultaneous removal of MB and Pb^{2+} from multi-component system.

Models	parameters	MB	Pb^{2+} ions
First order kinetic model:	K_1 (1/min)	0.287	0.195
$Log(q_e-q_t)=log(q_e)-(K_1/2.303)t$	q_e (cal) (mg/g)	5.89	29.04
	R^2	0.91	0.97
Second order kinetic model:	K_2 g/(mg min)	0.0791	0.0064
$t/q_t=1/K_2q_e^2 + (1/q_e)t$	q_e (cal) (mg/g)	42.194	24.030
	R^2	0.99	0.99
	h	140.84	3.74
Intraparticle diffusion	K_{diff} (mg/g $min^{1/2}$)	1.70	3.53
$q_t=K_{diff}\, t^{1/2}+C$	C (mg/g)	34.27	2.25
	R^2	0.61	0.90
Elovich	β (g/mg)	0.3501	0.1895
$q_t= 1/\beta \ln(\alpha\beta) + 1/\beta \ln (t)$	R^2	0.79	0.97
Experimental data	q_e(exp) (mg/g)	41.64	19.29

Table 7: Parameters of different Isotherms for Ru-NPs-AC multi-component system

Isotherm model	parameters	Pb^{2+} single	Pb^{2+} multi	MB single	MB multi
Langmuir	Q_m (mg g^{-1})	40.983	35.460	185.185	178.571
$C_e/q_e = 1/K_aQ_m + C_e/Q_m$	K_a (L mg^{-1})	0.129	0.030	4.153	4.000
	R^2	0.99	0.99	0.98	0.99
	R_L	0.0786-0.4058	0.3296-0.7469	0.0020-0.0157	0.0027-0.0163
$p_i = Q_m$ (single solute)/ Q_i (multi solute)	p_i		1.156		1.0370
Freundlich	1/n	0.381	0.341	0.461	0.445
Log q_e = log K_F+(1/n)log C_e	K_F (L mg^{-1})	8.59	8.75	151.33	138.89
	R^2	0.88	0.89	0.89	0.89
Temkin	B_l	8.51	7.07	32.09	27.28
$q_e = B_l \ln K_T + B_l \ln C_e$	K_T (L mg^{-1})	1.43	1.88	73.55	90.18
	R^2	0.96	0.94	0.96	0.97
Dubinin -	Q_s (mg g^{-1})	32.54	27.49	131.08	114.35
Radushkevich	B	3×10^{-6}	2×10^{-6}	2×10^{-8}	2×10^{-8}
$\ln q_e = \ln Q_s - B\varepsilon^2$	R^2	0.94	0.93	0.95	0.97